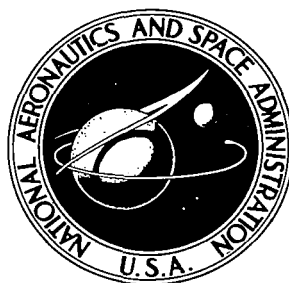


NASA TECHNICAL NOTE



NASA TN D-5627

c.1

NASA TN D-5627



LOAN COPY: RETURN :
AFWL (WLOL)
KIRTLAND AFB, N MEX

SIMPLIFIED METHOD FOR
CALCULATING THERMAL CONDUCTANCE
OF ROUGH, NOMINALLY FLAT SURFACES
IN HIGH VACUUM

by Daniel J. McKinzie, Jr.

*Lewis Research Center
Cleveland, Ohio*

NATIONAL AERONAUTICS AND SPACE ADMINISTRATION • WASHINGTON, D. C. • JANUARY 1970





01,32380

1. Report No. NASA TN D-5627	2. Government Accession No.	3. Recipient's Catalog No.	
4. Title and Subtitle SIMPLIFIED METHOD FOR CALCULATING THERMAL CONDUCTANCE OF ROUGH, NOMINALLY FLAT SURFACES IN HIGH VACUUM		5. Report Date January 1970	6. Performing Organization Code
		8. Performing Organization Report No. E-5293	
7. Author(s) Daniel J. McKinzie, Jr.		10. Work Unit No. 124-09	11. Contract or Grant No.
9. Performing Organization Name and Address Lewis Research Center National Aeronautics and Space Administration Cleveland, Ohio 44135		13. Type of Report and Period Covered Technical Note	
		14. Sponsoring Agency Code	
12. Sponsoring Agency Name and Address National Aeronautics and Space Administration Washington, D. C. 20546		15. Supplementary Notes	
16. Abstract A simplified approximate method for calculating the coefficient of thermal contact conductance has been derived. The method applies to the case of rough, nominally flat, outgassed surfaces in contact and under load in a high vacuum environment. The asperities of the surfaces are assumed to be undergoing plastic deformation. The method does not require the use of a computer program, but it does require the use of a surface analyzer and hardness tester. The method is used to calculate the interface conductance of two tungsten cylinders tested at approximately 10^{-6} torr and is in good agreement with experimental results.			
17. Key Words (Suggested by Author(s)) Thermal contact conductance Heat transfer Joint heat transfer Contact conductance		18. Distribution Statement Unclassified - unlimited	
19. Security Classif. (of this report) Unclassified	20. Security Classif. (of this page) Unclassified	21. No. of Pages 43	22. Price * \$3.00

*For sale by the Clearinghouse for Federal Scientific and Technical Information
Springfield, Virginia 22151

SIMPLIFIED METHOD FOR CALCULATING THERMAL CONDUCTANCE OF ROUGH, NOMINALLY FLAT SURFACES IN HIGH VACUUM

by Daniel J. McKinzie, Jr.

Lewis Research Center

SUMMARY

A simplified approximate method for calculating the coefficient of thermal contact conductance has been derived. The method applies to the case of two rough, nominally flat, outgassed surfaces in contact and under load in a high vacuum environment. The asperities of the surfaces are assumed to undergo plastic deformation. The method does not require the use of a computer program or the calculation of any abstract quantities. The surface parameters are obtained directly through the use of a surface analyzer and a microhardness tester. The derivation is based on the so-called "button" model of contact and is done by applying the basic steady-state Fourier heat conduction law written at the contact plane. An effective zone of the thermal disturbance is assumed to exist in the vicinity of the interface. The minimum length of this zone is assumed to be equal to the summation of the average of the maximum roughness heights of the two surfaces in contact.

The method is applied to an experiment involving two 2.54-centimeter-diameter tungsten cylinders. The cylinders are held in contact and under axial load in a vacuum environment of approximately 10^{-6} torr. The conductance was experimentally obtained as a function of the mean interface temperature at various constant contact pressures. However, the mathematical form of the experimental data was changed and plotted so that the effective area ratio of contact against contact pressure at constant interface temperature could be analyzed. This was done to demonstrate the change in the contact area with pressure that occurs during the history of such a contact. The agreement between the experimental results and theory is considered good.

A new technique for determining the variation of the specimen's contacting surface effective microhardness against temperature is also presented.

INTRODUCTION

The prediction of the coefficient of thermal contact conductance across metallic joints under load has received much attention during the past two decades, as indicated by references 1 to 17. Of particular interest is the work presented by Fenech and Rohsenow (ref. 2), Henry and Fenech (ref. 11), and Mikic and Rohsenow (ref. 15).

Fenech and Rohsenow (ref. 2) have considered the more general problem of deriving an expression for the thermal contact conductance of rough, nominally flat surfaces in contact as a function of the ambient fluid conductivity. As a limiting case, the authors considered the surfaces outgassed to a high vacuum. They chose the thermal conductivities of the specimen and the fluid filling the voids, the real area in contact, the number of contact points per unit cross-sectional area, and the volume average thickness of the void gaps as independent variables. These parameters have the shortcoming that they are not accessible to direct measurement but are only calculated or inferred from other measurements. Henry and Fenech (ref. 11) present a method for obtaining analog voltages of surface profiles of the contacting surfaces. They also present a general purpose analog computer program to determine the values of the geometric parameters of the contact interface (proposed by Fenech and Rohsenow) as a function of contact pressure. Thus, Henry and Fenech combine their computer program with the analysis of Fenech and Rohsenow. Mikic and Rohsenow (ref. 15) have treated the surfaces of contact as random processes with Gaussian distributions of height. They have considered four cases in particular. The solution they present for the case of rough, nominally flat surfaces in contact in a high vacuum environment is in a more simple form than that presented by Fenech and Rohsenow. The method of Mikic and Rohsenow requires the limited use of a computer in addition to the surface analyzer and surface microhardness tester. Though these analyses appear to have been experimentally confirmed by their authors, other investigators have found that the computerized programs outlined in references 2, 11, and 15 have required greater effort and cost than simply obtaining test data directly from sample specimens.

The investigators of references 2, 3, 5 to 7, 10 to 15, and 17 claim good experimental and theoretical agreement from their own experiment. The experimenters of references 1, 8, 10, and 13 have had difficulties in applying the theories of others to their test data. In part, this lack of agreement is believed due to the following:

- (1) There is insufficient knowledge of the microscopic and macroscopic structure of the specimen's contacting surfaces, where this knowledge is required to evaluate complex parameters appearing in the analyses.
- (2) There exists a lack of similarity between theoretical and experimental models.
- (3) Little or no consideration is given to the discrimination between elastic or plastic deformation phenomena that take place between the surface asperities of the test

specimen. If the conditions that bring about elastic or plastic deformation are not understood, their occurrence may become confused. This can happen, for example, if the experimenter inadvertently loads the asperities of his specimen well into their plastic deformation regime and then unloads them before gathering test data. The initial elastic phenomenon is obscured in this case because of the overshoot into the plastic regime where the microstructure of the surface asperities and properties of the surface material have changed irreversibly from their unloaded condition. Such an event may take place in the experimenter's attempt to align the test specimen interfaces. Thus, the initial elastic and plastic deformation phenomena would not be observed. An additional elasto-plastic problem may occur if the experimenter allows a change to take place in the mean interface temperature of his specimen during a test without considering the effect this change has on the hardness properties of the material.

Because of these problems and the complications introduced by the need for the computerized theoretical approaches of references 2, 11, and 15, the purposes of the present work are as follows:

(1) Reemphasis is made of the description of the elastic and plastic deformation of surface asperities on nonmoving surfaces in contact and under load as presented by Bowden and Tabor (no thermal effects included) in reference 18. This reemphasis is done to clarify the proper sequence of loading the interface so that meaningful experimental data can be obtained.

(2) Reemphasis is made of the importance of knowing the history of the contact joint.

(3) A new approximate method is presented for predicting the coefficient of thermal contact conductance for rough, nominally flat, outgassed surfaces undergoing plastic deformation in a high vacuum environment. This new method, which does not require a computer evaluation of the coefficient of thermal contact conductance, was derived by applying the basic steady-state Fourier heat conduction law to the so-called "button" model of contact.

(4) The new approximate method is applied to the interface of a tungsten-tungsten specimen tested in a high vacuum environment of approximately 10^{-6} torr, with ground surfaces of contact and approximately parallel lays.

(5) A new method is presented for determining the variation of the effective microhardness with temperature of the interface surface asperities.

MECHANICAL CONTACT PHENOMENON

The following discussion of the mechanical contact phenomenon, which is presented in greater detail in reference 18, consists of a description of the mechanical aspects of the loading, work hardening, and unloading of a surface asperity. This discussion is

included because it describes the reversible and irreversible events occurring during the making of a contact. It also demonstrates the importance of knowing the history of the contact event.

Loading of an Asperity

Reference 18 considers an idealized case where the tip of an asperity is assumed to be smooth and spherical in shape. A single asperity is assumed to rest on a softer metal, and, in the region of contact, the surface of the softer metal is considered to be a plane (see fig. 1(a)). Consider what happens as the load on the asperity is increased in three steps.

First, if the surface asperity is pressed into the plane with a load W' , it at first deforms elastically according to Hertz's classical equations. (All symbols are defined in appendix A.) At this stage, the planar projection of the area of contact A'_c ($A'_c = \pi a^2$) is proportional to $W'^{2/3}$, since from Hertz's equation written for a flat surface being penetrated by a single spherical asperity

$$a = 1.1 \left[\frac{W' r}{2} \left(\frac{1}{E_1} + \frac{1}{E_2} \right) \right]^{1/3} \quad (1)$$

where a is the radius of the contact indent (see fig. 1(b)), r is the initial radius of curvature of the asperity, and E_1 and E_2 are Young's moduli for the two surfaces, respectively. In this range the deformations are reversible.

Second, as the load is increased, the mean pressure p_m (i. e., $p_m = W'/A'_c$) over the contact area of the asperity increases until it reaches such a value that at a critical point z (see fig. 1(c)) within the softer metal the elastic limit is exceeded. From reference 18, the Hertzian analysis indicates this region is situated at a point about $0.6a$ below the center of the area of contact. At this stage the metal reaches a state of plasticity and yields irreversibly. The metal outside the vicinity of point z has not yet reached the conditions for plasticity, so its deformation is still essentially elastic.

Third, as the load is increased further, the area of contact A'_c and the mean pressure p_m rise in a manner which deviates increasingly from the elastic relation. The region of plasticity at point z below the center of the area of contact grows rapidly, and a stage is soon reached at which the whole of the metal around the region of contact is flowing plastically (see fig. 1(d)). At this condition, the theoretical works of Hencky and of Ishlinsky mentioned in reference 18 show that

$$p_m = cY \quad (2)$$

where Y is the elastic limit of the softer metal as found in pure tension, and c has a value of approximately 3.

Work Hardening of an Asperity

Bowden and Tabor (ref. 18) consider the effects of work hardening in an attempt to describe the change of A'_c with increased p_m . They point out that all metals experience work hardening during increased loading. As before, they assume a hard smooth spherical asperity penetrates the surface of a smooth softer metal. Their assumed sequence of events is now described.

As a load is applied, the formation of an indentation produces an increase in the elastic limit Y of the surface metal. It follows from this result that when metal surfaces rest on one another the peaks of their asperities readily deform plastically with the mean pressure given by equation (2). The parameter Y in equation (2) is some "representative" measure of the elastic limit of the deformed metal at the tip of the asperities, and c depends on the shape and size of the surface irregularities. The coefficient c has a value of about 3 for hemispherical asperities and for conical and pyramidal asperities over a wide range of angles.

With conical and pyramidal asperities the yield pressure is independent of the amount of deformation that has occurred. Thus, the area of real contact A'_c is directly proportional to the load W' . With hemispherical asperities this is only true for metals whose surfaces are highly work hardened.

For all the surfaces considered herein the surface asperities are assumed to be highly work hardened by the grinding process used to prepare them. Therefore, for all types and shapes of surface irregularities, the real area of contact A'_c is considered proportional to the load in the plastic regime. Thus,

$$A'_c \propto W' \quad (3a)$$

or

$$\frac{A'_c}{A} \propto p' \quad (3b)$$

where

$$p' = \frac{W'}{A}$$

and A is the total cross-sectional area of the surface considered.

Unloading of an Asperity

Next, the unloading of the surface asperity is considered. From reference 18, in the range of initial elastic deformation, the process of deformation is completely reversible. Hence, a removal of the load enables the contacting surfaces to return to their original configurations.

For the case of initial plastic deformation of a single asperity, consider a hard sphere of radius a penetrating a softer metal under a load W'_0 to form an indentation of diameter d' (circular planar projection of the indent). Suppose the load W'_0 on the sphere is removed and then replaced. The indentation should now be in exactly the same condition as when it was originally plastically formed. Thus, any change which has occurred in the configuration of the surface between removing and replacing the indenter over the same loading range must be reversible; that is, it must be elastic. Consequently, the recovered (unloaded) indentation has a radius of curvature larger than that of the spherical indenter. At any stage in this process, if the load is reduced, there is a relaxation of elastic stresses, and the area over which the surfaces touch is given by the laws of elastic deformation. It should be pointed out that this statement does not imply that equation (1) still holds. Specifically, equation (1) is written for a single asperity penetrating a flat plate and not for a single asperity penetrating a surface which is concave, as would be the case here. It does, however, imply that an indentation diameter d' is reached at the stage where the load returns to the value W'_0 and the elastic deformation has reached its end. The whole of the surface is in a stage of incipient plasticity, and, if the load is increased by a small amount, further plastic deformation occurs and the indentation increases in size.

The process of loading and unloading an asperity is described graphically in figure 2, which is similar to a figure given in reference 18. Figure 2 indicates that, as the load on a single asperity is increased, an initial elastic deformation of the area of contact occurs; this is predicted by equation (1). At some larger load the onset of plastic deformation takes place, and the variation of the area of contact A'_c with load is then predicted by the approximate equation (eq. (2)) for plastic deformation. If the asperity is then unloaded at some higher load W'_0 and area of contact $A'_{c,0}$, the variation of the area of contact against load is indicated by the dashed curve labeled reversible elastic deformation. If, further, the load on the asperity is removed, an offset in the area of contact $A'_{c,1}$ due to plastic deformation will occur, as shown in figure 2.

THEORETICAL ANALYSIS

The object of this analysis is to determine an approximate parametric relation for the coefficient of thermal contact conductance written for two rough, nominally flat,

outgassed surfaces in contact in a high vacuum environment, where the asperities on these surfaces are undergoing plastic deformation. The analysis is based on the steady-state Fourier one-dimensional heat conduction law. It is applied to the so-called "button" model of contact described in reference 2. A discussion of the experimental determination of the quantities appearing in the derivation is included. Also included is a parametric relation between the coefficient of the thermal contact conductance and the contact pressure for the unloading of an interface.

Coefficient of Thermal Contact Conductance for Plastic Regime

Figure 3 is a view of the assumed contact interface showing a contact region labeled the effective zone of the thermal disturbance. The length of this zone is assumed to include the sum of the largest asperity roughness heights of both portions of the specimen. This height is used as the best measurable length approximating the physical length of the zone of thermal disturbance. Because this length may be smaller than the actual length over which the thermal discontinuity at the interface takes place, it is referred to here as the effective zone of the thermal disturbance.

Assumptions. - The following assumptions must be applicable to the test specimen before the parametric relations developed in this work may be used:

- (1) The ends of the cylindrical specimen are nominally flat (as defined in ref. 6). The surface features are measured in microinches and defined in reference 19.
- (2) Plastic deformation of the asperities in contact is taking place.
- (3) The surfaces are clean and outgassed to a high vacuum environment.
- (4) The contacting cylinders are made of the same material.
- (5) Effects of creep are negligible across the interface of contact.
- (6) Effects of radiation are negligible across the interface of contact.
- (7) The outside walls of the specimen are adiabatic.
- (8) The axial length of the effective zone of the thermal disturbance δ is very small compared to the specimen's diameter.

The following assumptions apply to the theoretical model which is used to approximate the specimen.

- (1) The specimen's contacting surface asperities are each replaced by the so-called "button" model of contact.
- (2) Each button contact is thermally insulated from its neighbor.
- (3) The number of button contacts is uniformly distributed over the interface of contact.
- (4) The axial temperature distribution in each cylinder of a button contact is the same as every other one. Thus, their circular areas of contact may be summed. The

resulting single area of contact is shown in figure 4 (modified from ref. 2) and shall hereafter be referred to as "the button contact."

(5) The face of the button contact is in a state of plastic deformation with increasing load.

(6) No thermal gradient exists in the radial direction of the cylindrical button contact.

(7) The axial temperature gradient is constant and remains steady in time throughout the cylindrical volume of the button contact.

(8) The length of the effective zone of the thermal disturbance is very small and is equal to the sum of the lengths of the button contacts of the upper and lower portions of the model. It is therefore assumed that only within the effective zone of the thermal disturbance does the thermal discontinuity at the interface exist and that the thermal gradient in this zone is constant and steady in time. This concept is unique to the present analysis.

(9) The interface of contact between the button contacts is located at a point one-half the axial length of δ (see fig. 5). This assumption is made though the lengths of the button contacts δ_1 and δ_2 shown in figure 4 are not necessarily equal. This relocation does not introduce an error into the theoretical analysis because the length of δ is assumed to be very small. Thus the change in the mean temperature of the interface of contact (fig. 4) is negligible.

(10) Outside the effective zone of the thermal disturbance the temperature distribution is steady in time throughout the cylindrical model.

Analysis. - When these assumptions are applied to the model, the axial temperature distribution in the vicinity of the interface is as shown in figure 5. The basic steady-state one-dimensional Fourier heat conduction law written for the effective zone of the thermal disturbance δ (figs. 4 and 5) is given by

$$\frac{\dot{Q}}{A_c} = -k \frac{dt}{dx} \quad (4)$$

where A_c is the sum of the individual cross-sectional areas of the idealized individual "button" contacts, and k is the coefficient of thermal conductivity. This coefficient is evaluated at a temperature equal to $(t_{i,1} + t_{i,2})/2$ (see fig. 5), and dt/dx is the axial temperature gradient across the disturbance zone δ .

If equation (4) is applied to the effective zone of the thermal disturbance (see fig. 5), the heat-transfer rate per unit area at the interface of contact may be approximated by

$$\frac{\dot{Q}}{A} = \frac{-k \Delta t_c}{\delta} \quad (5)$$

where from figure 5 at $x = -x_1$

$$t = t_{\textcircled{1}} \quad (6)$$

and at $x = x_2$

$$t = t_{\textcircled{2}} \quad (7)$$

Thus,

$$\Delta t_c = t_{\textcircled{2}} - t_{\textcircled{1}} \quad (8)$$

and equation (5) becomes

$$\frac{\dot{Q}}{A_c} = -k \frac{(t_{\textcircled{2}} - t_{\textcircled{1}})}{\delta} \quad (9)$$

The coefficient of thermal contact conductance h is defined in the equation

$$\frac{\dot{Q}}{A} \equiv -h \Delta t \quad (10)$$

where A , the cross-sectional area of the specimen, is expressed by

$$A = \pi R^2 \quad (11)$$

If the temperature gradients in the specimen outside the effective zone of the thermal disturbance are linearly extrapolated to the interface $x = 0$, as shown in figure 5, then Δt at the interface is given by

$$\Delta t = t_{i,2} - t_{i,1} \quad (12)$$

Substituting equation (12) into equation (10) gives

$$\frac{\dot{Q}}{A} = -h(t_{i,2} - t_{i,1}) \quad (13)$$

Equating the heat-transfer rate \dot{Q} across the interface, equations (9) and (13), yields

$$kA_c \frac{(t_{\textcircled{2}} - t_{\textcircled{1}})}{\delta} = Ah(t_{i,2} - t_{i,1}) \quad (14)$$

From figures 4 and 5 and equations (8) and (12),

$$|\Delta t_c| \geq |\Delta t| \quad (15)$$

Since δ is very small, it is reasonable to assume

$$|\Delta t_c| = |\Delta t| \quad (16)$$

Substituting equations (8) and (12) into equation (16) yields

$$t_{\textcircled{2}} - t_{\textcircled{1}} = t_{i,2} - t_{i,1} \quad (17)$$

Equation (14) thus reduces to

$$h \frac{\delta}{k} = \frac{A_c}{A} \quad (18)$$

From plastic theory for nominally flat surfaces in contact (ref. 2),

$$\frac{A_c}{A} = \frac{P}{I} \quad (19)$$

where P is the pressure resulting from the applied load W acting over the total nominally flat surface πR^2 , and I is the average of the random microhardness values of the softer of the two interface surfaces. Substituting equation (19) into equation (18) results in the desired relation

$$h \frac{\delta}{k} = \frac{P}{I} \quad (20)$$

Unloading the Contacting Surfaces

Consider the case of unloading the contacting surfaces from some plastically deforming pressure P_0 at a constant mean interface temperature where $P_0 = (W_0/\pi R^2)$. Equation (1) can be applied to the summation of the individual contact areas. Therefore,

$$A_c \propto W^{2/3} \quad (21)$$

Multiplying equation (21) by $1/A$ yields

$$\frac{A_c}{A} \propto \frac{W^{2/3}}{A} \quad (22)$$

where A is πR^2 . If some upper load W_o is set as a limit, the area of contact $A_{c,o}$ has the same magnitude for the elastic and plastic regime. Substituting equation (18) into proportionality (22) at load W_o results in

$$\frac{h_o \delta}{k} \propto \frac{W_o^{2/3}}{A} \quad (23)$$

or

$$\frac{h_o \delta}{k} \propto \frac{P_o^{2/3}}{A^{1/3}} \quad (24)$$

In the elastic regime at a constant mean interface temperature assume

$$\frac{\delta}{k} = C \quad (25)$$

where C is a constant. If now the interface is unloaded from P_o to P_1

$$\frac{(hC)_o}{(hC)_1} = \frac{\left(\frac{P^{2/3}}{A^{1/3}}\right)_o}{\left(\frac{P^{2/3}}{A^{1/3}}\right)_1} \quad (26)$$

where $A_o = A_1$ and $C_o = C_1$. Equation (26) thus reduces to

$$h_1 = \left(\frac{P_1}{P_o}\right)^{2/3} h_o \quad (27)$$

Substituting equation (20) into equation (27) yields

$$h_1 = P_1^{2/3} P_o^{1/3} \frac{k}{\delta I_o} \quad (28)$$

or substituting equation (18) into equation (27) yields

$$\left(\frac{A_c}{A}\right)_1 = \left(\frac{P_1}{P_o}\right)^{2/3} \left(\frac{A_c}{A}\right)_o \quad (29)$$

Thus equation (28) provides a method for calculating the coefficient of thermal contact conductance for any point below the upper limit of P_o and h_o . This is true if the mean interface temperature of the contacting surfaces and the heights of the plastically deformed asperities remain constant or very nearly constant during the unloading processes.

EXPERIMENTAL APPARATUS AND PROCEDURE

Test Apparatus

Sketches of the bell jar, its contents, and its location in the test setup are shown in figures 6 and 7. Simply, the test is performed in a bell jar that contains an induction heating coil and a column composed of the test specimen, a heat meter, and heat sink as shown in figure 6. A pneumatic loading cylinder is located on top of the bell jar as shown in figure 7. The loading cylinder is used to vary the pressure at the contact interface of the test specimen. Electrical currents are induced in the extreme upper portion of the test specimen. The heat generated by these currents is transferred across the test interface, through the heat meter, and finally to the water-cooled heat sink. The test specimen and heat meter are instrumented with thermocouples. The millivolt level output of the thermocouples is read out on a potentiometer. The bell jar operates at a vacuum condition in the 10^{-6} torr range. A detailed discussion of the test apparatus and specimen is given in appendix B.

Experimental Determination of h

The experimental method used to determine the coefficient of thermal contact conductance h of a tungsten-tungsten interface is given in this section.

Test procedure. - The coefficient of thermal contact conductance of the tungsten-tungsten specimen was experimentally determined using equation (13) and the test apparatus described in appendix B. Heat was transferred from a source across the tungsten-tungsten interface of contact and then to a heat sink (see fig. 6). The rate of heat transfer across the interface was determined with the aid of an oxygen-free high-conductivity (OFHC) copper heat meter. The test specimen was designed so that a one-dimensional linear heat-transfer analysis would apply. Thus the hypothetical Δt of equation (10) was experimentally determined by a linear extrapolation of the thermal gradients from the upper and lower portion of the specimen to the interface (see fig. 5).

Before proceeding it should be stated that the sequence of changes made in pressure and temperature were not ideally made throughout the test. For the first 22 runs, out of a total of 72, the data were obtained by correctly varying the test conditions. As noted in figure 8, these data were obtained by correctly increasing the pressure between successive testing periods in which the interface temperature was changed in a monotonic increasing manner. Thus changes in the area of contact due to elastic or plastic effects taking place with a rise in interface pressure and/or temperature were distinctly obtained. The data of figure 8 were subsequently cross plotted in figure 9 with the aid of equation (18). Figures 10 and 11 present the data of figure 9 in varying degrees of refinement.

Three power failures occurred during the test resulting in four subgroups of data, as noted in figure 11. However, the contact pressure remained constant during each of them. The first two interruptions occurred after runs 12 and 32 when the interface temperatures were approximately 331 and 382 K, respectively. And the third occurred after run 36 when the interface temperature was 529 K. After each interruption the test specimen cooled to room temperature before power was reapplied. Thus differences in lateral contractions resulted in sliding among the asperities.

The shortest period of time needed to establish steady-state conditions after a change was made in pressure was approximately $1\frac{1}{2}$ hours. The average time required was $2\frac{1}{2}$ hours. Changes in interface temperature were made in a minimum time of 3 hours, with the maximum being 48 hours. These intervals of time were considered adequate based on previous experience. However, better steady-state data would have been obtained with finer control of the power.

The interface surfaces were cleaned with acetone before installation in the test facility. In future tests the necessity for using some standard cleaning procedure seems apparent, because of the possibility of film deposition from such a solvent as acetone.

Data reduction. - The upper piece of the test specimen (fig. 6) was instrumented with six special type Chromel-Alumel 30 gage wire thermocouples. The lower piece was instrumented with five thermocouples. Six more were located in the OFHC copper heat meter at three axial stations. The value of the thermal conductivity used to com-

pute the heat transfer across the heat meter was obtained from data presented in reference 20 and is shown in figure 12. Figure 13 demonstrates a typical best line fit drawn through the experimental thermocouple data. The linear extrapolation of these data was used to determine the interface temperature difference. Two typical runs, runs 13 and 23, are shown. The thermocouple readings at the 3.2 millimeter locations on either side of the specimen's interface were omitted from consideration. This was done because of the constrictive resistance effects (ref. 15) taking place in the vicinity of the interface. A further simplification was made in the data reduction by determining the thermal gradient in each portion of the specimen from two thermocouple readings in the same manner as that used by Fried (ref. 2). The gradients determined by this technique were continually checked by plots such as that of figure 13. This simplified procedure used the same thermocouples throughout the tests. Thus, an added degree of consistent variation in the data resulted with varying input heating rates. The error in the temperature difference across the interface introduced by this method was generally less than 1.1 K from a best line fit through all the thermocouple data. However, the manufacturer's accuracy tolerance of ± 1.1 K must apply in an error analysis because a calibration of the thermocouples on the specimen was not made. It should be mentioned that the large temperature difference, Δt , obtained across the interface during the majority of test runs helped to minimize the error introduced by using Fried's first-order fit. The smallest value of Δt was 9 K which occurred at a mean interface temperature of 331 K and a pressure of approximately 5.31×10^6 newtons per square meter. This occurred for 1 run out of the total of 72. The next smallest Δt was 18.3 K which also occurred only once. The largest value of Δt , 250 K, occurred at a mean interface temperature of 666 K and a pressure of approximately 4.83×10^5 newtons per square meter.

Theoretical Determination of h

The value of h was determined from values of δ , k, and I together with equation (20). The quantities δ and I were evaluated from the test specimen. The variation with temperature of tungsten's thermal conductivity k, which was estimated from the literature (ref. 21), is presented in figure 14.

Measurement of the effective zone of the thermal disturbance δ . - A Brush Surfanalyzer was used to determine the magnitude of δ . It consists of a control unit, a stylus 1200 drive unit, a 50-milligram stylus probe, and a recorder unit. This apparatus records the surface roughness (width and height), profile, waviness, and arithmetic average height. All of these quantities are defined in reference 19.

During the approach of two rough, nominally flat surfaces the maximum roughness height would make contact first. Therefore, it is appropriate to determine the average

value of the maximum roughness heights δ_1 (upper) and δ_2 (lower) of the test specimen before the test is made. Since it is not possible to obtain surface analyzer traces which include all the points of contact on a surface, a representative number of traces must be taken. From each of these traces, a single value of the maximum roughness height is obtained. These values are then averaged to obtain the value of the roughness height used in the calculations. The value of δ , where $\delta = \delta_1 + \delta_2$, shall hereafter be referred to as the effective value of the thermal disturbance height. For the test reported here the magnitudes of δ_1 and δ_2 (5.35 and 5.51 μm), respectively, were determined by averaging the maximum roughness heights obtained from six traversals at different positions on each face of the specimen perpendicular to their ground lay.

In the test reported here the magnitudes of δ_1 and δ_2 were determined after the test data were obtained. This occurred because the instrumentation required to determine δ_1 and δ_2 was not available before the test was performed. Ideally, the maximum roughness height should be determined from the specimen before the conductance test is started. If, however, the test is completed before the traces are obtained, references 2 and 22 indicate that the roughness heights will be only slightly smaller. This is only true, however, if full plastic flow of the cylindrical specimen is far from being approached. The loads applied and of interest in the test considered here, and most other contact conductance investigations, satisfy this condition. In references 2 and 22 the specimen's roughness height did not decrease further after its initial plastic deformation even though much larger loads were applied.

As shown in figures 8 and 11, the arithmetic average roughness heights for the upper and lower surfaces were 0.538 and 0.943 micrometer, respectively.

Measurement of the Microhardness

As pointed out in reference 3, the microhardness of cold-rolled nickel and mild steel contact surfaces was up to five times larger than their Meyers hardness value determined from a 1.905-centimeter-diameter cylinder. Specifically, the microhardness increased as the load on the microhardness indenter decreased from 4.44×10^4 to 0.444 newton. Reference 3 indicates that Laming (ref. 23) observed an apparent increase of the microhardness with decrease in the indenter loading for steel-brass and steel-aluminum test specimens. Reference 11 also indicates an increase in the microhardness of a surface as the indenter load is decreased.

The test reported here has also indicated an increase in the value of the contact surface microhardness as the indenter load is decreased. The increase in microhardness was obtained with a Knoop indenter at room temperature and is shown in figure 15. The choice of the Knoop indenter used in this test was based on the advantages of its use that were mentioned in reference 24. The increase in surface microhardness is attributed to

surface work hardening caused by the method of surface preparation (in this test, ground). This increase has proved to be of great importance. As pointed out in reference 11, the correct value of the microhardness is that value obtained when the hardness indenter penetrates to the same depth that an asperity penetrates the specimen's surface. However, the depth of asperity penetration is a difficult measurement to make. Because the penetration depth of the Knoop indenter is geometrically related to the length of its major and minor diagonals, these observed indents may also be used as a measure of the depth of indenter penetration. This is done by comparing at the same magnification a metallograph photograph of the microhardness tester indents at various loads with one of the asperity indents. The larger diagonal of the Knoop indenter is best used as an indicator of the penetration depth. This is because the included angle of the indenter which forms the major diagonal is approximately $172\frac{1}{2}^{\circ}$, which is more closely equal to the included angle of most characteristic asperities (160° to 164° , ref. 6). This range of included angles has also been confirmed by our experience.

Although this technique of making the indenter penetration comparable to the asperity is desirable, it could not be used entirely in the test reported here. This was because the Tukon microhardness tester used had a minimum Knoop indenter load of 0.245 newton. At this load the larger diagonal indicated the indenter penetration depth varied from about two to five times greater than the average asperity indent. However, the value of the hardness determined with this load was used in the analysis. The variation of the microhardness with indenter load is presented in figure 15.

Effect of Temperature on Hardness

The tensile strength, thus the hardness, and recrystallization of the tungsten specimen are functions of temperature (ref. 25). Therefore, it is important to include the effect of temperature on the hardness in the calculation of the theoretical value of the coefficient of thermal contact conductance. The variation of the specimen's surface microhardness with temperature was not obtained from microhardness data. However, it is suggested that this variation may be determined by applying the subsequent procedure. If it is assumed that (1) the specimen's interface asperities are kept under a constant pressure as the mean interface temperature is raised and (2) the average value of the maximum roughness height of each portion of the specimen remains constant during the change in temperature, then equation (20) reduces to

$$\frac{h_1}{h_2} = \frac{\left(\frac{k}{I}\right)_1}{\left(\frac{k}{I}\right)_2} \quad (30)$$

where the subscripts 1 and 2 refer to different temperatures at which data is taken. Thus, the variation of k/I with temperature can be obtained as a function of the conductance. If the thermal conductivity of the specimen is known as a function of temperature, the variation of an effective microhardness with temperature can be obtained. Thus,

$$\left(\frac{I_1}{I_2}\right)_{\text{eff}} = \frac{k_1}{k_2} \frac{h_2}{h_1} \quad (31)$$

The procedure is best done after the variation of the coefficient of thermal contact conductance with pressure, at constant interface temperature, has been obtained. And the data are best obtained at test conditions slightly higher in pressure and temperature than the largest values of these variables used to obtain the conductance data. This is because equation (31) is written for the plastic deformation regime. Also it is important to keep the specimen's interface temperature well below the temperature of recrystallization if the specimen is not 100 percent recrystallized. This restriction is important because the change in grain boundaries that occurs during recrystallization may have adverse effects on the transmission of heat across them.

The technique was applied to the data of runs 7 to 11 indicated in figure 8 at a pressure of 5.31×10^6 newtons per square meter. Substituting the variation of the thermal contact conductance and thermal conductivity with temperature into equation (31) results in the variation of the specimen's effective surface microhardness with temperature as shown in figure 16, curve A. This curve is referenced to the microhardness obtained at room temperature and shown in figure 15 ($8.72 \times 10^9 \text{ N/m}^2$). The values of the effective microhardness used to determine the curves and points labeled as plastic theory in figure 11 were taken from figure 16, curve A. The data of curve B, taken from reference 26, approximate those of curve A as noted from figure 16.

DISCUSSION OF RESULTS

The original purpose of the experiment was to show how the coefficient of thermal contact conductance for two rough, nominally flat, outgassed surfaces in contact and under load varied with changes in the mean interface temperature of the specimen. The

contact conductance data were obtained at interface pressures of 4.83×10^5 , 2.55×10^6 , and 5.31×10^6 newtons per square meter (fig. 8). At the time the experiment was performed it was not realized that a monotonic increase of interface pressure and/or temperature was the ideal procedure for obtaining data for a specimen. This scheme of testing is necessary because of the unique elastic and plastic deformation phenomena that occur only during the first loading cycle. These phenomena are thus associated with the history of changes in loading and/or temperature of the asperities in contact. Not all of the test data presented here were obtained by the ideal variation of pressure and temperature. However, the data resulting from the nonideal experimental procedures used clearly show effects which are explained by theoretical considerations. In turn, these results indicate the importance of knowing the history of the changes through which the asperities go.

The data, which are shown in figure 8, are cross-plotted in figure 9 with the aid of equation (18). Figures 10 and 11 present the data of figure 9 in varying degrees of refinement. The data of figure 8 were replotted because their form was not easily related to the description of the contact phenomena presented here and shown graphically in figure 2. Therefore, figures 9 to 11 are plots of the effective area ratio of contact against contact pressure. These figures indicate that, at a constant interface temperature, deformation ranging from plastic to elastic took place during the loading or unloading, respectively, of the tungsten-tungsten specimen. This deformation range supports the description given in reference 18.

The data of figure 8 were obtained in a timewise sequence of five distinct groups. Each group consists of data obtained by varying the specimen's interface temperature from a lower to an upper limit. The strict maintenance of constant interface pressure for each data group was not considered important at the time the data were obtained. Thus, some of the data include small pressure and thermal variations. This testing technique induced unwanted effects in the data and would not be used at present. It was during the first 22 runs (fig. 8) that both the highest pressure and temperature levels were imposed on the specimen. Thus, the initial elastic and plastic deformation of the test specimen occurred during these runs.

The first timewise group of data, A to B, shown as the lowest curve in figure 9 has a distinctly different slope of the effective area ratio of contact against increasing pressure than the remaining groups. Also, the magnitude of the slope for the first group agrees with plastic theory, while the slope for the remaining groups appear to agree with the elastic theory, though this is not clearly discernible in figure 9.

Figure 10, which is an attempt to present more clearly the conductance data than is done in figure 9, is a plot of selected data from figure 8 at the specific interface temperatures of approximately 378, 392, 529, 570, 628, and 666 K. These temperatures were chosen because of the availability of data at two or three pressures. The data of fig-

ure 10 indicate the slope of the three point pressure data (approximately 4.83×10^5 , 2.55×10^6 , and 5.31×10^6 N/m²) is generally not constant with pressure. The slope of the data in the supposedly elastic region appears to vary from the anticipated theoretical value of 2/3, while the slope of the data between runs 1 and 6 (at an interface temperature of approximately 390 K) agrees closely with the value of 1 from plastic theory. Thus a somewhat confused picture of just what is happening at the specimen's interface of contact with changes in pressure and temperature would result from only considering the data presented in figure 10.

Figure 11, which is a refinement of the data presented in figure 10, presents only data obtained after the specimen is believed to have reached thermal equilibrium; in addition, possible effects due to several power failures that occurred during the test period are eliminated. Three power failures occurred which resulted in four unique subgroups of data. The power failures occurred at interface temperatures of approximately 331, 382, and 529 K after runs 12, 32, and 36, respectively. After each, the specimen cooled to room temperature while the contact pressure remained constant. The cause of these power failures is not known. Because of the likelihood that microscopic lateral asperity misalignments took place, due to large interface differential temperature effects, it is assumed that the data for each of these groups is independent of the others. The curves of figure 11 result by joining like temperature data in each of the subgroups. Separating the data in this manner results in slopes for the curves that agree well with plastic or elastic theory.

The variation of the surface microhardness with temperature is necessary to calculate the effective area ratio of contact for the plastic regime shown in figure 11. This variation in microhardness is normally obtained by indenter techniques; however, it may be obtained using a new technique which will be described. The specimen's microhardness may be calculated as a function of temperature by substituting the experimental data of figure 8, the thermal conductivity from figure 14, and a reference value of the specimen's microhardness into equation (31). The reference value of the microhardness (8.74×10^9 N/m²) was obtained by indenter techniques at approximately 294 K and is presented in figure 15. The resulting variation of the specimen's effective microhardness with temperature (curve A) is presented in figure 16. Also included in figure 16 are tungsten hardness data obtained from thin sheet (0.025 cm) highly cold worked high purity tungsten having no stress relief (ref. 25) and 0.071-centimeter-diameter drawn high purity tungsten wire (ref. 26). These curves were obtained by converting the yield strength data presented in these references into hardness data. The conversion was done by multiplying the yield strength by the usual coefficient of 3. It should be pointed out that the temperature range of the data presented in figure 16 is well below the recrystallization temperature of tungsten and also below the temperature range of stress relief. Therefore, the difference in hardness levels is due to the degree of cold working of the

tungsten material. It is noted that the slopes of all three curves are approximately equal. Thus it appears that curve A represents the hardness variation of the surface asperities of the tungsten specimen with temperature. Because of the good agreement in magnitude and slope between the hardness data of curves A and B (ref. 26), the curves and points of figure 11 labeled plastic theory were determined by using equation (19) where the value of the microhardness was taken from curve A (fig. 16). The agreement is considered good between the theoretically calculated and experimentally determined values of the effective area ratio of contact against pressure presented in figure 11. It is believed that the use of this technique for predicting the variation of the effective microhardness of a contact interface is unique to this report.

As a further check on the plastic theory represented by equation (20), a calculation of the thermal contact conductance was made at a pressure of 5.31×10^6 newtons per square meter and an interface temperature of 294 K (room temperature). The hardness value of 8.74×10^9 newtons per square meter was obtained from microhardness indenter data (fig. 15), and the conductivity was obtained from figure 14. The value of the calculated conductance ($9.11 \text{ kW}/(\text{m}^2)(\text{K})$) is approximately 15 percent larger than that obtained from the conductance experimental data shown in figure 8 ($h_1 = 7.93 \text{ kW}/(\text{m}^2)(\text{K})$). This experimental value was obtained by extrapolation of the data for runs 6 to 11 to an interface temperature of 294 K. These data were used because they are believed to be the result of pure plastic deformation of the specimen's interface surfaces of contact. Most of the remaining data in figure 8 are believed the result of elastic deformation; therefore, equation (20) cannot be used with these data to predict the coefficient of thermal contact conductance.

The elastic data shown in figure 11 were obtained at interface pressures below the maximum impressed during the initial plastic deformation of the asperities. The magnitude of the slopes agrees well with the elastic theoretical value of $2/3$, as noted in figure 11.

A small error study was performed to indicate the reliability of the theoretical and experimental results. The error introduced into the effective area ratio of contact varied from approximately -6 percent (below) to 11 percent (above) the theoretical values. This is due to the known scatter in the microhardness of the softer of the specimen's surfaces of contact (see fig. 15). The effect of this scatter on the plastic theoretical curve is shown in figure 11 at a mean interface temperature of 390 K.

No accurate estimate of the error in the effective area ratio of contact for the experimental data could be made. This was due to the lack of thermocouple and thermal conductivity calibration data of the tungsten-tungsten specimen. The calculation of the experimental error was made with the aid of references 20, 21, and 27. When conservative estimates of the errors are made, the largest error in the effective area ratio of contact varied from -18 percent (below) to 10 percent (above) the experimental values.

This error, however, applied to only three runs out of the total of 72. The next closest estimate of the error resulted in a variation from -11.3 percent (below) to -0.6 percent (below) the experimental values for a total of 10 runs. And the majority of runs had a variation from -8.2 percent (below) to -1.6 percent (below) the experimental values. Thus, the majority of the data had a mean error of approximately -5 percent (below) the experimental values.

Radiation losses affecting the accurate determination of heat transfer across the interface of contact were found to be negligible at all test conditions.

CONCLUSIONS

The following are concluded from this study:

1. A new simplified approximate theoretical method is presented (eq. (20)) for predicting the coefficient of thermal contact conductance. It applies to the case of two rough, nominally flat, outgassed surfaces in contact and plastically deforming in a high vacuum environment. The method does not require the use of a computer program. It does, however, require the use of a surface analyzer and a microhardness tester. The analysis is based on an application of the one-dimensional steady-state Fourier heat conduction law to the interface of contact of an idealized "button" contact. An effective zone of the thermal disturbance is assumed to exist in the vicinity of the interface. The zone's minimum length is assumed to be equal to the summation of the average of the maximum roughness heights of the two surfaces in contact. These assumptions are unique to this method.

2. The importance of knowing the entire history of events that the test surfaces experience during their engagement is emphasized. Thus, meticulous care of the specimen must be taken. Also, a carefully prepared program of experimentation must be made and followed to achieve meaningful results. The importance of monotonically increasing pressure and/or interface temperature has been pointed out. And the necessity for uninterrupted testing has been made obvious from the experimental results reported here.

3. An experiment is performed using a tungsten-tungsten specimen tested in a vacuum environment of 10^{-5} to 10^{-6} torr. The results of this test are compared with theoretically anticipated results. The agreement is considered good though several deficiencies in the experimental method are pointed out. While the deficiencies in experimental method have been pointed out herein, it must also be mentioned that similar deficiencies have probably been overlooked in some previous studies. A relation predicting the variation of the coefficient of thermal contact conductance during the contact disengagement (elastic regime) has been presented. The coefficient may be calculated if the maximum pressure at which the contacting surfaces are compressed is known and their mean inter-

face temperature remains constant as the pressure is reduced. Also, a relation has been presented between the elastic variation of the effective area ratio of contact and decreasing pressure.

4. A new technique for determining the variation of the effective microhardness of the interface surface asperities with temperature has been presented. This technique has been applied to the tungsten experimental data obtained in the present study. The resulting variation of the effective hardness with temperature is shown to agree with hardness data in the literature. This technique must be applied after the experimental variation of the conductance with pressure has been obtained.

Lewis Research Center,
National Aeronautics and Space Administration,
Cleveland, Ohio, October 23, 1969,
124-09.

APPENDIX A

SYMBOLS

A	total cross-sectional area of cylindrical model, m^2	p_m	mean pressure on a single asperity, $p_m = W'/A'_c$, N/m^2
A_c	summation of individual areas of button contacts (results in total area of actual contact), m^2	\dot{Q}	rate of heat transfer, W
A'_c	contact area of one asperity, πa^2 , m^2	R	radius of the cylindrical model, m
a	asperity radius of contact, m	r	radius of curvature of the asperities in contact, m
C	constant	t	temperature, K
c	constant in $p_m = cY$	Δt	extrapolated temperature difference across the interface of contact, K
d	diameter of asperity contact, $d = 2a$, m	Δt_c	temperature difference across the effective zone of the thermal disturbance, K
d'	diameter of planar projection of indent resulting from penetration of a flat surface by a spherical indenter	W	applied load acting over the total nominally flat surface, N
E	Young's modulus of elasticity, N/m^2	W'	load applied to asperity in contact, N
h	coefficient of thermal contact conductance, $kW/(m^2)(K)$	W_o	upper value of loading in plastic range of softer metal (load acting over total nominally flat surface), N
I	microhardness, N/m^2	W'_o	upper value of asperity loading in plastic range of softer metal (see fig. 2), N
k	coefficient of thermal conductivity, $W/(m)(K)$	x	length from interface of button contacts along axis of cylinders (see fig. 4), m
P	total load applied to specimen divided by entire cross-sectional area, N/m^2	Y	elastic limit in tension, N/m^2
p'	load applied to one asperity divided by the total cross-sectional cylindrical area, $p' = w'/A$, N/m^2		

δ effective zone of the thermal disturbance or average of the maximum roughness heights of a surface, m

Subscripts:

c plane of button contact

eff effective

i interface

o condition of maximum loading
(see fig. 2)

1, 2, } stations or offset in area of
①, ② } contact

APPENDIX B

DISCUSSION OF APPARATUS

The test apparatus was designed specifically for investigating the thermal contact conductance problem. A stainless steel bell jar encloses the test chamber. (Stainless steel was used for reasons of safety and cleanliness.) The jar rests on a base plate and on an instrument ring which contains eight vacuum feedthroughs (see fig. 6). An observation port located in the bell jar cover allows viewing of the test specimen contact plane and some 5.08 centimeters beyond on either side of it. The cover is fastened by bolts to the base plate on which an electrically insulated, water cooled, copper heat sink rests. A pneumatic loading cylinder (fig. 7) supplies a constant force, denoted by W in figure 6, to the cylindrical specimen. The loader is fastened to the top of the bell jar by four long stemmed studs which complete a closed force system between the loading cylinder and the specimen.

A small hammer assembly (fig. 7) is used to overcome the static friction of two stationary O-ring seals that are located in the top of the bell jar and are in contact with the circumference of the loading cylinder heat shield (fig. 6). The hammer is actuated intermittently by an electric solenoid through a motor-driven cam and switch. A hand-operated hoist located over the facility provides easy removal of the bell jar cover.

A vacuum of 10^{-5} to 10^{-6} torr was maintained in the bell jar during the test. This operating condition should be adequate for simulating space conditions. Reference 16 indicates that (1) the convection of heat conducted to air begins to decrease at approximately 70 torr and measurably disappears at 10^{-1} torr, and (2) other investigators have stated that a vacuum in the range of 10^{-4} torr is sufficient to negate the conduction effect of interstitial fluids.

Vacuum System

The vacuum system is composed of a 15.24-centimeter oil diffusion pump, a mechanical holding pump, high vacuum valves, and the necessary vacuum instrumentation. A liquid nitrogen cold trap is located in the high vacuum line between the diffusion pump and the bell jar high vacuum valve. The cold trap inhibits the backstreaming of diffusion pump oil into the bell jar. The vacuum measuring instrumentation consists of a thermocouple - ionization gage control.

Feedthroughs

Eight feedthrough ports allow flexibility in the system. Two of these are used for the passage of water-cooled copper tubes which are connected to the induction coil. Another set of copper cooling lines lead to the copper water-cooled heat sink shown in figure 6. A third feedthrough, not shown in figure 6, is used to connect a small liquid-nitrogen cryopump to a liquid nitrogen system. The cryopump consists of a 2.54-centimeter-outside-diameter copper finned tube 12.7 centimeters long which protrudes into the bell jar. A fourth feedthrough is used for installation of an ionization gage. All of the feedthroughs are sealed to the instrument ring with O-rings.

Test Specimen and Column

The following is a consideration of the column of apparatus which includes the test specimen. In descending order, this column consists of a pneumatic loader, load cell, hammer and solenoid, loading cylinder, induction coil, specimen, heat sink, and base plate as shown in figures 6 and 7.

Loader. - The loader (fig. 7), which is a pneumatic cylinder containing a piston and shaft, is used to load the specimen so that data may be obtained as a function of the interface pressure. Air pressure is applied to the loader by a controller containing a solenoid actuated valve which allows air pressure to be applied to either side of the piston. The solenoid is actuated by a toggle switch on the control panel (fig. 7). The magnitude of the pressure is regulated by a pressure regulator with a range 0 to 8.61×10^5 newtons per square meter. The regulator controls the pressure in the piston to within about 350 newtons per square meter. This pressure is read out on a direct reading gage which has an accuracy of approximately 500 newtons per square meter.

Load cell. - The load or force on the interface of the specimen is determined by the compression of a load cell. The load cell is located between the shaft of the loader and the loading cylinder which passes from the outside to the inside of the bell jar. The load cell was calibrated by the deadweight method from 0 to 9.52×10^2 newtons. The calibration was extended to 6.275×10^3 newtons through use of a materials testing machine and had an accuracy of approximately ± 1 newton per square centimeter. The bridge voltage of the load cell was maintained at 1.001 volts. This voltage was supplied by an external battery supply and rheostat and was measured with the aid of a Rubicon Potentiometer. The output voltage of the load cell was read on a nonovoltmeter which had a range from 0.1 microvolt to 100 millivolts. Two additional external forces had to be taken into account to determine the total true load on the test interface. These forces consisted of (1) the weight of the loading cylinder, load cell, and the upper portion of the test speci-

men (figs. 6 and 7), and (2) the force due to atmospheric pressure acting on the load cylinder which has a cross-sectional area of approximately 20.3 square centimeters. The additional weight due to these forces amounted to 2.44×10^2 newtons. This force resulted in a pressure of 4.82×10^5 newtons per square meter acting on the interface of contact in addition to the pressure applied pneumatically.

Heater coil. - The method used to heat the specimen is of vital concern in a successful test. An inductive heating unit was adapted to the test apparatus and specimen arrangement. The inductive coil had 10 turns of hollow copper tubing having an overall outside coil diameter of approximately 8.25 centimeters (fig. 6). The coil was water cooled from a central manifold which was supplied by city water. The inductive source was a 10 080-hertz motor-generator set, which is rated for 220 volts at 136 amperes or approximately 30 kilowatts at 0 kilovars. Although the actual input power throughout the tests varied from approximately 600 watts to 2.9 kilowatts, this piece of equipment maintained a regulated level of output power within approximately ± 3.5 percent. The heat transferred across the test specimen's interface of contact was varied from 7 to 400 watts during the test. Since tungsten is nonferrous and has a magnetic permeability of approximately 1.000068 times that of free space, the magnetic field produced by the induction coil was unaffected by the test specimen's presence. At the center of the coil's axis, the magnetic field reached a maximum value of approximately 3.06×10^{-5} tesla during the test. Though the field induced currents in the vicinity of the specimen's interface, their effect was negligible. The effect of the induction coil's magnetic field on the thermocouples was also negligible. This was because the leads from each thermocouple were twisted for some distance away from the zone of the coil and specimen and had no loops in them.

To make use of the existing inductive heating source, the upper portion of the test specimen was made long enough so that the contact plane of the interface was 8 centimeters below the lower turn of the inductive heating coil. The specimen's upper portion extended approximately 4 centimeters above the coil where it came in contact with a 1.90-centimeter-diameter sapphire sphere.

Specimen. - The test specimen was metallurgically prepared from high purity pressed and sintered tungsten powder. Its 2.54-centimeter-diameter cylindrical configuration was specified because of one-dimensional heat-transfer considerations. The specimen's upper portion was 25.4 centimeters long so that it passed completely through the 10 turns of the induction heating coil. The lower portion of the specimen was 2.54 centimeters long (fig. 6).

Surface finish. - The lay of the specimen's interface surfaces was produced by grinding. The average value of the maximum roughness height across the lay of the upper and lower surfaces was 5.35 and 5.51 micrometers, respectively, and their arithmetic average roughness heights were 0.538 and 0.943 micrometer, respectively. These values were determined after the test was completed. The test was performed

with the lay of the top and bottom surfaces approximately parallel. It was found that the maximum waviness height (defined in ref. 16) of the surfaces was less than the average value of the maximum roughness height. This fact supports the assumption that the specimen surfaces were nominally flat.

Interface temperature and pressure range. - Space environmental conditions of interest determined the choice of interface temperatures at which the data were obtained. Reference 16 indicates that the range of greatest interest extends from 200 to 589 K. Because the present investigation only extended upwards from room temperature, the values of 394 and 589 K were chosen as minimum and maximum interface temperatures, respectively, for the present tungsten-tungsten tests. As noted in figure 8 the actual test range extended from approximately 350 to 739 K for the three interface contact pressures of 4.83×10^5 , 2.55×10^6 , and 5.31×10^6 newtons per square meter.

Thermometry. - For the design temperatures of 394 to 589 K, a choice of thermocouple materials had to be made. The special type Chromel-Alumel thermocouple wire was selected both because of its high millivolt output and its nearly linear voltage variation with temperature in the range of interest. These thermocouples have an accuracy of ± 1.1 K as guaranteed by the manufacturer in the range of temperatures from 273 to 550 K, and $\pm 3/8$ of 1 percent from 550 to 1533 K. The thermocouples were fabricated from 30 gage thermocouple wire twisted at its ends and welded. They were then peened into holes 0.32 centimeter deep in the surface of the cylinders. The thermocouple leads were sheathed in glass insulation. Upon exiting from the holes the leads were wound around one-half the specimen's circumference. Several small hanger straps fastened to the model on one end located the leads on the circumference of the specimen. The first straps were located approximately 1.27 centimeters from the holes to prevent interference with the thermal response of the thermocouples in the holes. The output of each thermocouple was read on a Rubicon portable potentiometer, which can accurately be read to three significant figures and a fourth can be approximated.

As shown in figure 6, six thermocouples were located on the upper and five on the lower portion of the specimen. Also three sets of two thermocouples 180° apart were located on the OFHC copper heat meter. A calibration was not made of the thermocouples on the specimen and heat meter. However, figure 13 shows a typical plot of the specimen temperature against axial distance, where the readings are generally constant with x over moderate temperature ranges. From plots similar to figure 13 the thermocouples were shown to vary within the manufacturers' indicated tolerance for the special type of Chromel-Alumel wire used. The data from thermocouple locations 0.32 centimeter on either side of the interface were not included in the data reduction. This was done because they were believed affected by the thermal discontinuity of the interface. Reference 28 was used to reduce the raw thermocouple data.

Heat meter. - As shown in figure 6, a 6.35-centimeter oxygen-free high conductivity

(OHFC) copper heat meter was located between the lower portion of the test specimen and the copper heat sink. The heat-transfer rate through the test specimen was determined from the heat meter experimental data. The curve of thermal conductivity against temperature used to reduce the copper heat meter data is shown in figure 12. The data were obtained from reference 20.

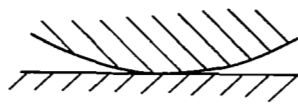
Heat sink. - As shown in figure 6, the heat meter is screwed into a copper water-cooled heat sink. The heat sink contains two internal cooling channels. The maximum difference between the inlet and outlet water temperature to the heat sink was estimated to be less than 1 K during the test.

The heat sink rests on a 0.32-centimeter thick electric insulator which, in turn, rests on the base plate of the bell jar (fig. 6). The electric insulator plus the electrical isolation of the water lines leading to the heat sink inhibited an external current system from being established between the bell jar and the specimen column.

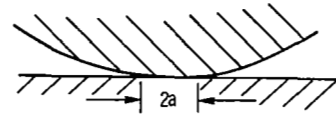
REFERENCES

1. Fried, Erwin: Study of Interface Thermal Contact Conductance. Rep. 66SD4471, General Electric Co. (NASA CR-82778), July 31, 1966.
2. Fenech, H.; and Rohsenow, W. M.: Prediction of Thermal Conductance of Metallic Surfaces in Contact. Heat Transfer, vol. 85, no. 1, Feb. 1963, pp. 15-24.
3. Williams, A.: Heat Transfer Through Metal to Metal Joints. Proceedings of the Third International Heat Transfer Conference. Vol. 4. AIChE, 1966, pp. 109-117.
4. Anon.: Proceeding of Conference on Thermal Joint Conductance. NASA TM X-56300, 1964.
5. Ozisik, M. N.; and Hughes, D.: Thermal Contact Conductance of Smooth-To-Rough Contact Joints. Paper 66-WA/HT-54, ASME, Nov. 1966.
6. Yovanovich, M. Michael; and Fenech, H.: Thermal Contact Conductance of Nominally-Flat, Rough Surfaces in a Vacuum Environment. Thermophysics and Temperature Control of Spacecraft and Entry Vehicles. Vol. 18 of Progress in Astronautics and Aeronautics. G. B. Heller, ed., Academic Press, 1966, pp. 773-794.
7. Yovanovich, M. Michael: Thermal Contact Conductance in a Vacuum. Rep. DSR-4542-39, Massachusetts Inst. Tech. (NASA CR-74619), Nov. 1965.
8. Bloom, M. F.: Thermal Contact Conductance in a Vacuum Environment. Rep. SM-47700, Douglas Aircraft Co., Inc. (NASA CR-75148), Dec. 13, 1964.
9. Graff, W. J.: Thermal Conductance Across Metal Joints. Machine Design, vol. 32, Sept. 15, 1960, pp. 166-172.
10. Clausing, A. M.: Heat Transfer at the Interface of Dissimilar Metals - The Influence of Thermal Strain. Int. J. Heat Mass Transfer, vol. 9, no. 8, Aug. 1966, pp. 791-801.
11. Henry, J. J.; and Fenech, H.: The Use of Analog Computers for Determining Surface Parameters Required for Prediction of Thermal Contact Conductance. J. Heat Transfer, vol. 86, no. 4, Nov. 1964, pp. 543-551.
12. Holm, R.: Thermal Conduction Through Nominally Flat Metallic Contacts in Vacuum Environment. Stockpole Carbon Co., 1965.
13. Clausing, A. M.; and Chao, B. T.: Thermal Contact Resistance in a Vacuum Environment. Rep. ME-TN-242-1, Univ. Illinois Eng. Experiment Station, 1963.

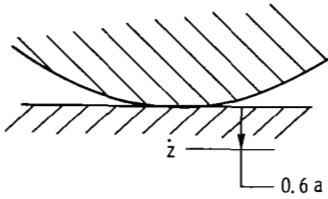
14. Cetinkale, T. N.; and Fishenden, M.: Thermal Conductance of Metal Surfaces in Contact. International Conference on Heat Transfer. Inst. Mech. Engrs., London, 1951, pp. 271-275.
15. Mikic, Borivoje B; and Rohsenow, Warren M.: Thermal Contact Resistance. Rep. 4542-41, Mass. Inst. Tech. (NASA CR-78319), Sept. 1966.
16. Smuda, P. A.; Fletcher, L. S.; and Gyrog, D. A.: Heat Transfer Between Surfaces in Contact: The Effect of Low Conductance Interstitial Materials. Part I: Experimental Verification of NASA Test Apparatus. Rep. ME-TR-033-1, Arizona State Univ. (NASA CR-73122), June 1967, p. 55.
17. Fenech, Henri; and Rohsenow, W. M.: Thermal Conductance of Metallic Surfaces in Contact. Rep. NYO-2136, Heat Transfer Lab. Mass. Inst. Tech., May 1959, pp. 42-54.
18. Bowden, F. P.; and Tabor, D.: The Friction and Lubrication of Solids. Clarendon Press, Oxford, 1950, pp. 5-24.
19. Anon.: Surface Texture, Surface Measurement. USA Standards Inst., B46.1-1962.
20. Lucks, C. F.; and Deem, H. W.: Thermal Properties of Thirteen Metals. Spec. Tech. Pub. 227, ASTM, 1958.
21. Anon.: Thermophysical Properties Research Center Data Book. Vol. I - Metallic Elements and Their Alloys. Purdue Univ., 1960, Fig. 1029, curve nos. 9 and 14.
22. Kragelsky, I. V.; and Demkin, N. B.: Contact Area of Rough Surfaces. Wear, vol. 3, 1960, pp. 170-187.
23. Laming, L. C.: Thermal Conductance of Machined Metal Contacts. International Developments in Heat Transfer. ASME, 1963, pp. 65-76.
24. Williams, Samuel R.: Hardness and Hardness Measurements. ASM, 1942, pp. 199-204.
25. Anon.: Product Data Sheet 1400-C. General Electric Co., Lamp Metals and Components Dept., Aug. 12, 1963, pp. 1411-1412.
26. Lyman, Taylor, ed.: Properties and Selection of Metals. Vol. 1 of Metals Handbook. Eighth ed., ASM, 1961, p. 1226.
27. Touloukian, Y. S., ed.: Thermophysical Properties of High Temperature Solid Materials. Vol. I: Elements. Macmillan Co., 1967, pp. 458, 466, 1025, 1031.
28. Shenker, Henry; Lauritzen, John I., Jr.; Corruccini, Robert J.; and Lonberger, S. T.: Reference Tables for Thermocouples. Circ. 561, National Bureau of Standards, Apr. 27, 1955.



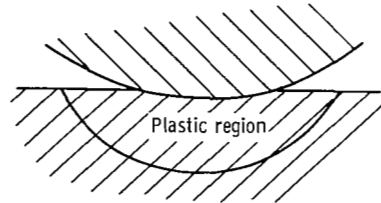
(a) Spherical asperity resting on a plane surface.



(b) Elastic deformation of the contact joint.



(c) Incipient plastic deformation of the contact joint.



(d) Plastic deformation of the contact joint.

Figure 1. - Progressive deformation of a plane surface by spherical asperity.

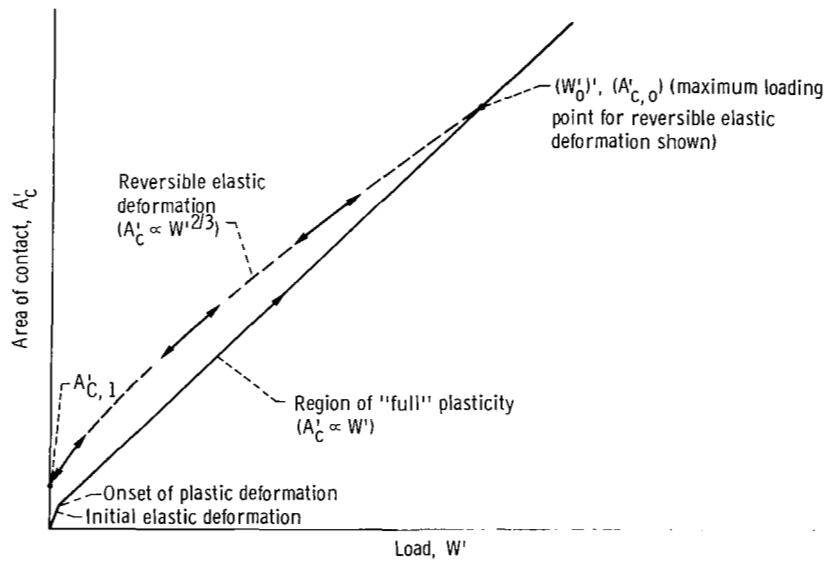


Figure 2. - Area of contact as function of load for increasing and decreasing load application to a single asperity indenting a flat plate (ref. 18).

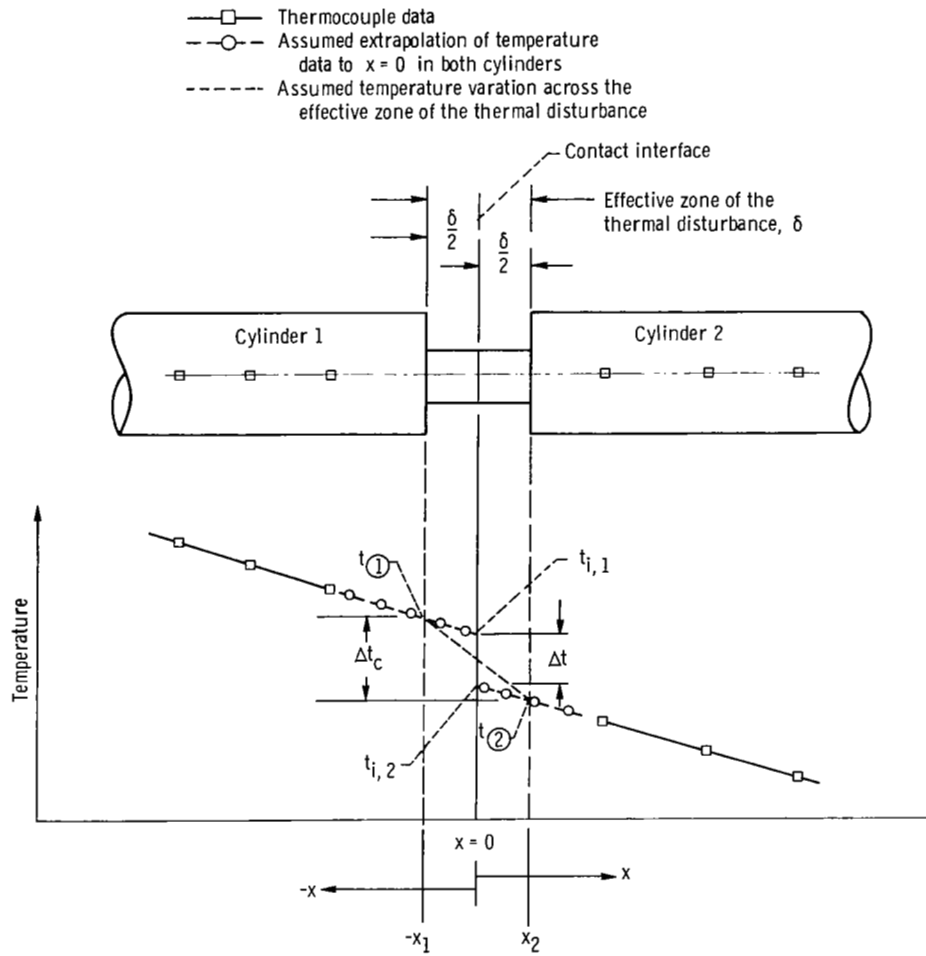


Figure 5. - Temperature profile along specimen.

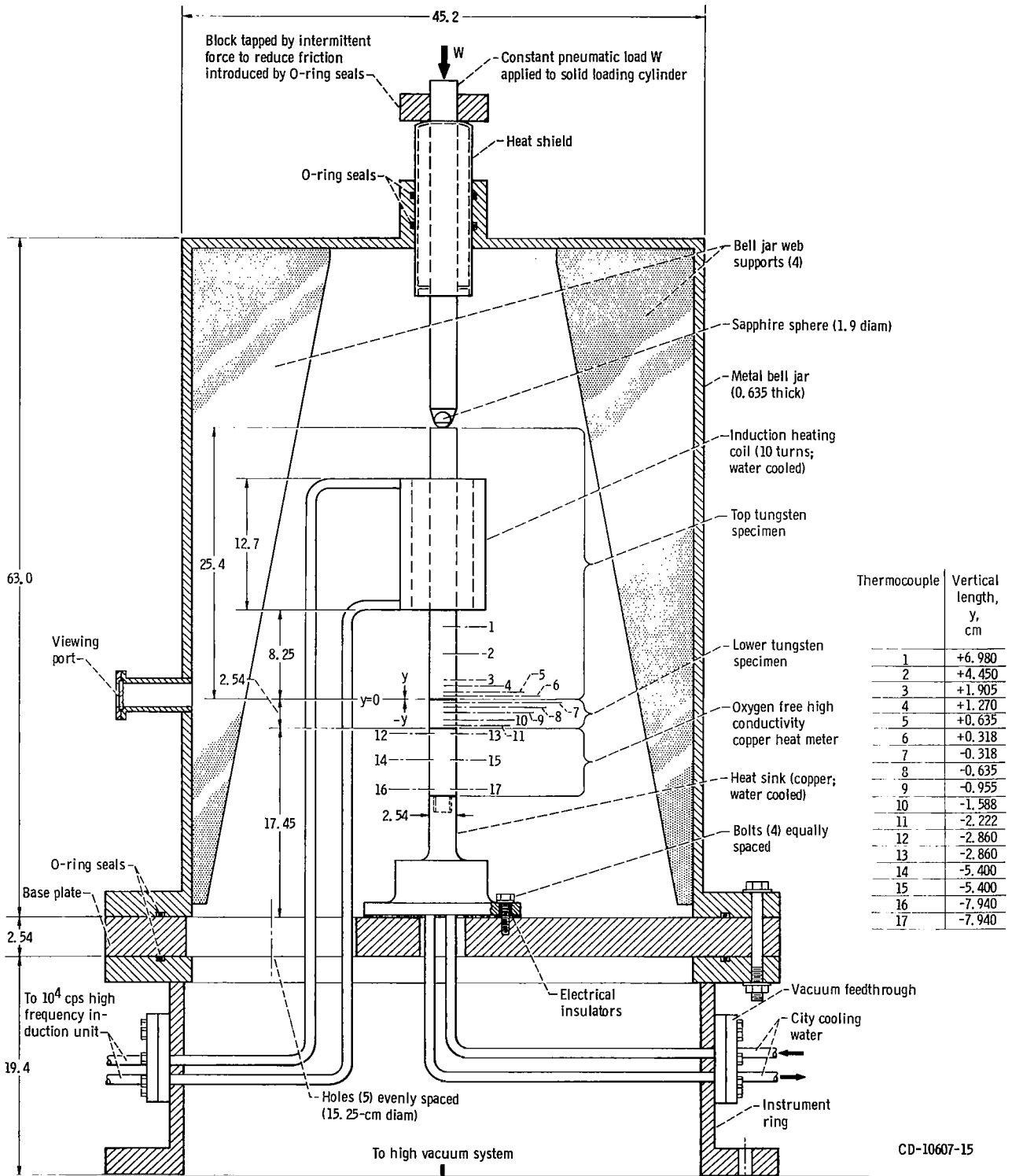
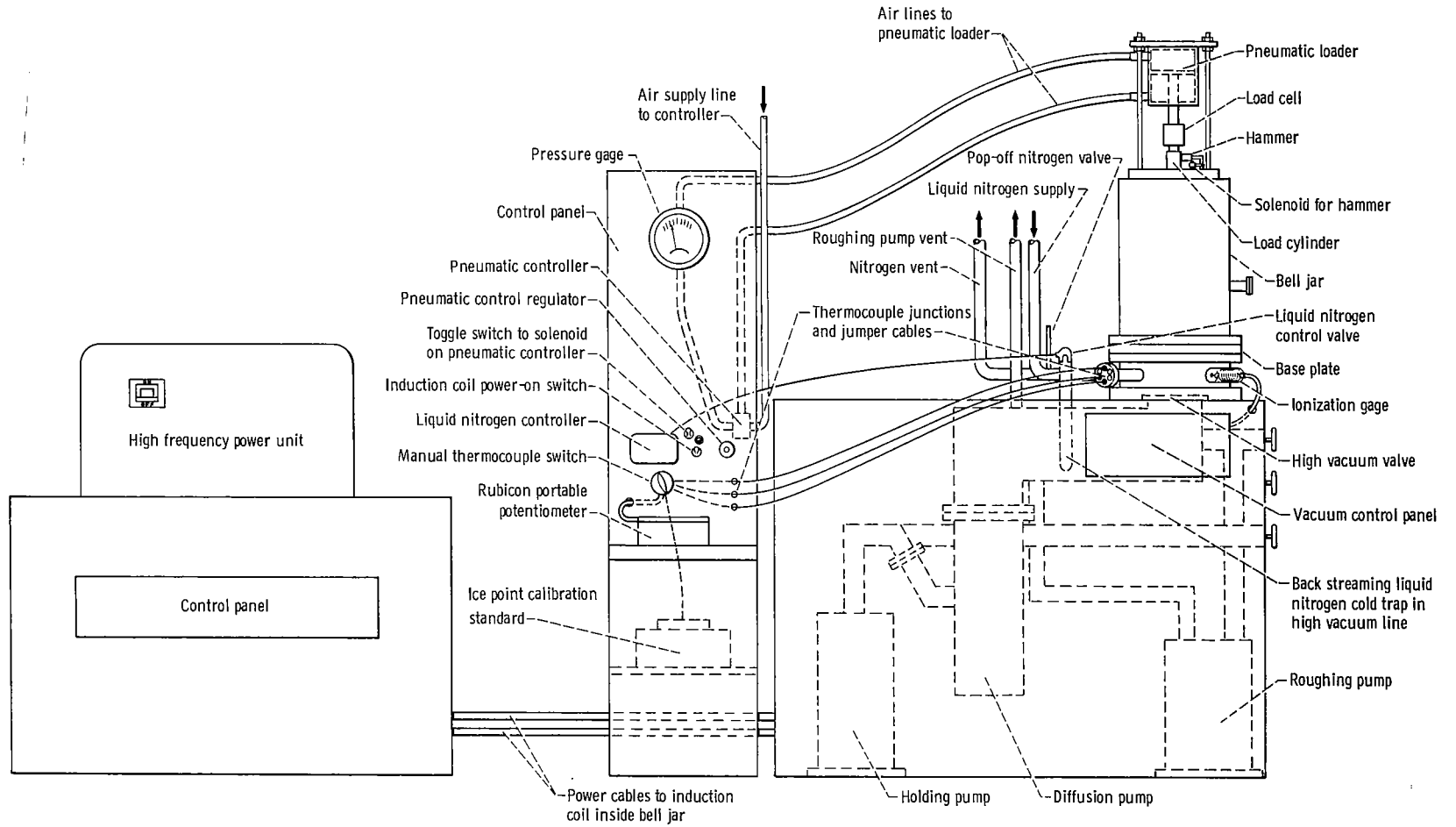


Figure 6. - Internal view of bell jar. (All dimensions are in cm.)



CD-10606-15

Figure 7. - High vacuum equipment facility, bell jar, control equipment, and power supply.

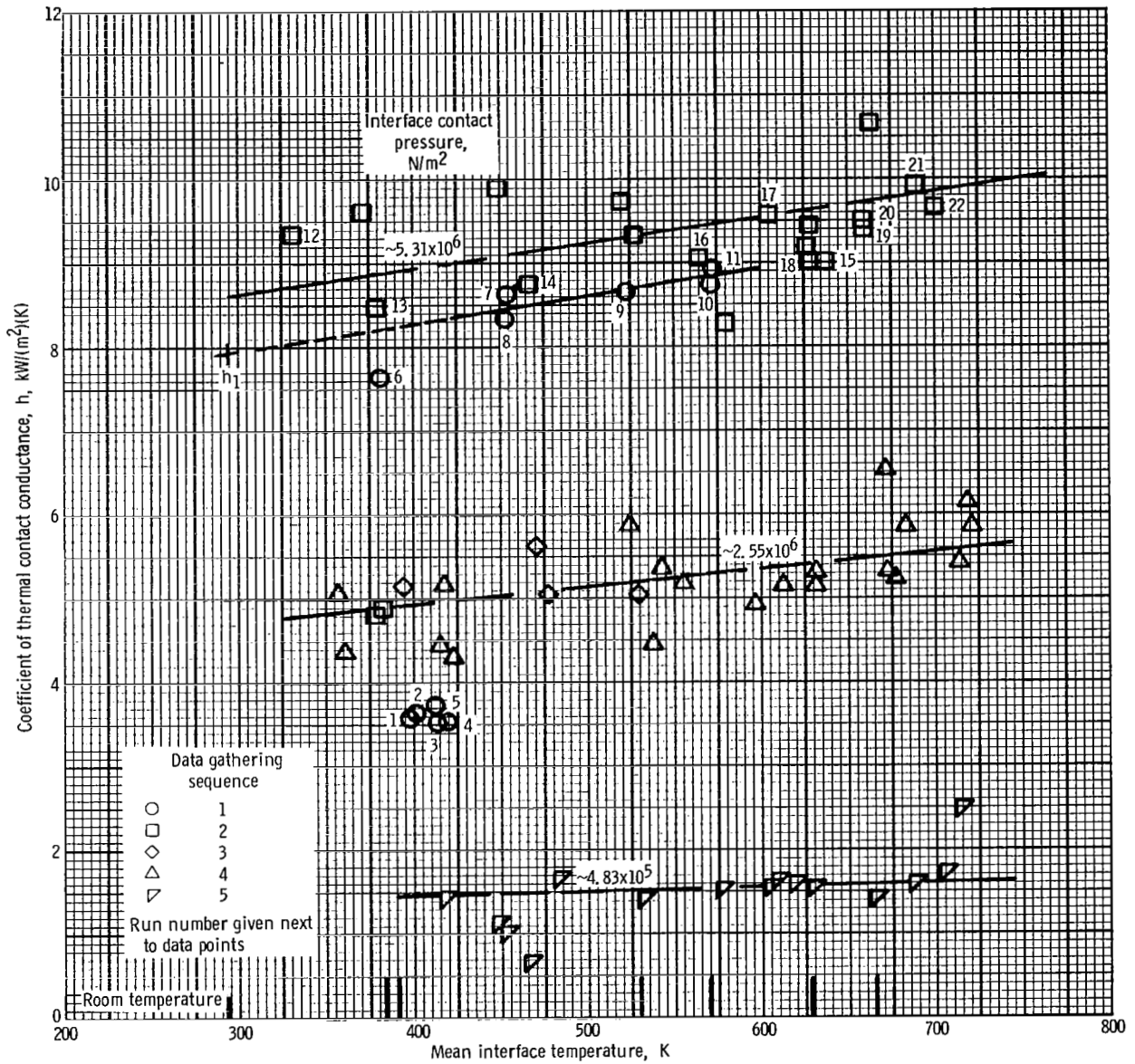


Figure 8. - Tungsten-tungsten coefficient of thermal contact conductance data as function of temperature for ground surfaces with approximately parallel lays. Arithmetic average roughness heights for upper and lower surfaces are 0.538 and 0.943 micrometer, respectively.

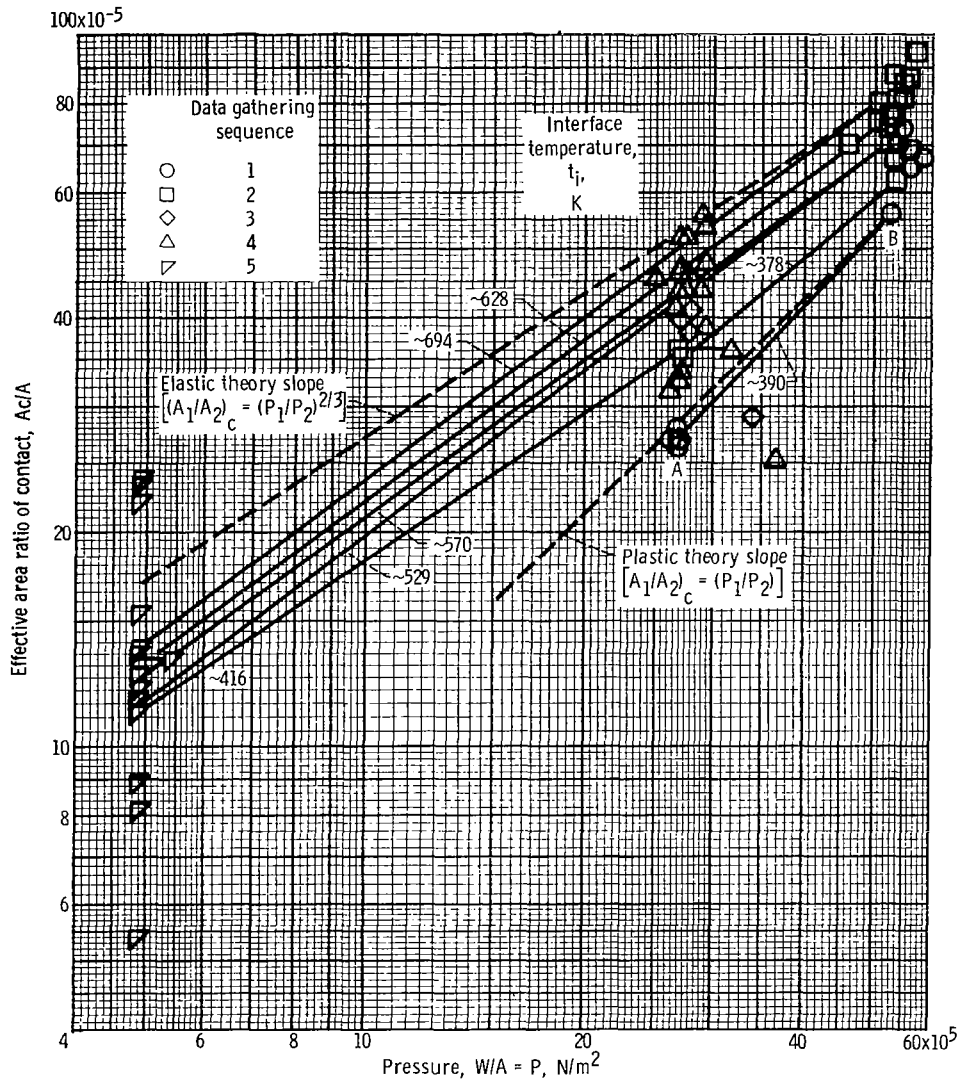


Figure 9. - Tungsten-tungsten data of figure 8 replotted as effective area ratio of contact against pressure.

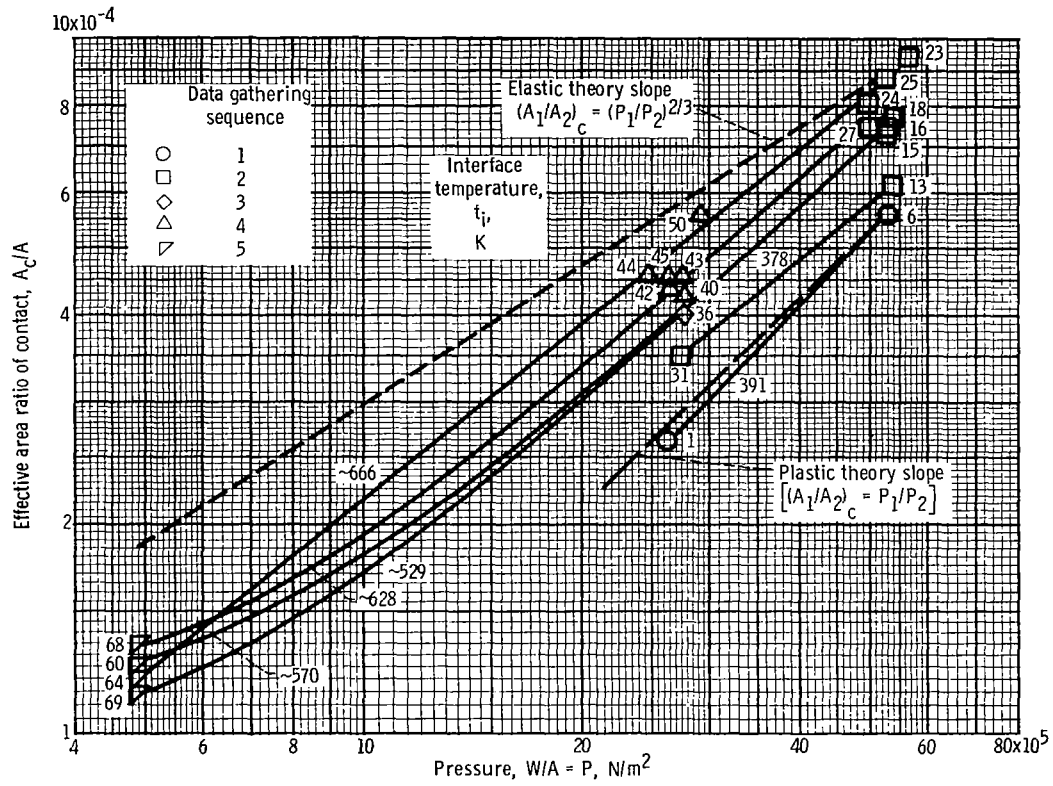


Figure 10. - Selected two and three point tungsten-tungsten data of figure 8 replotted without regard to power interruptions. Demonstrates possible misinterpretation of data in plastic regime.

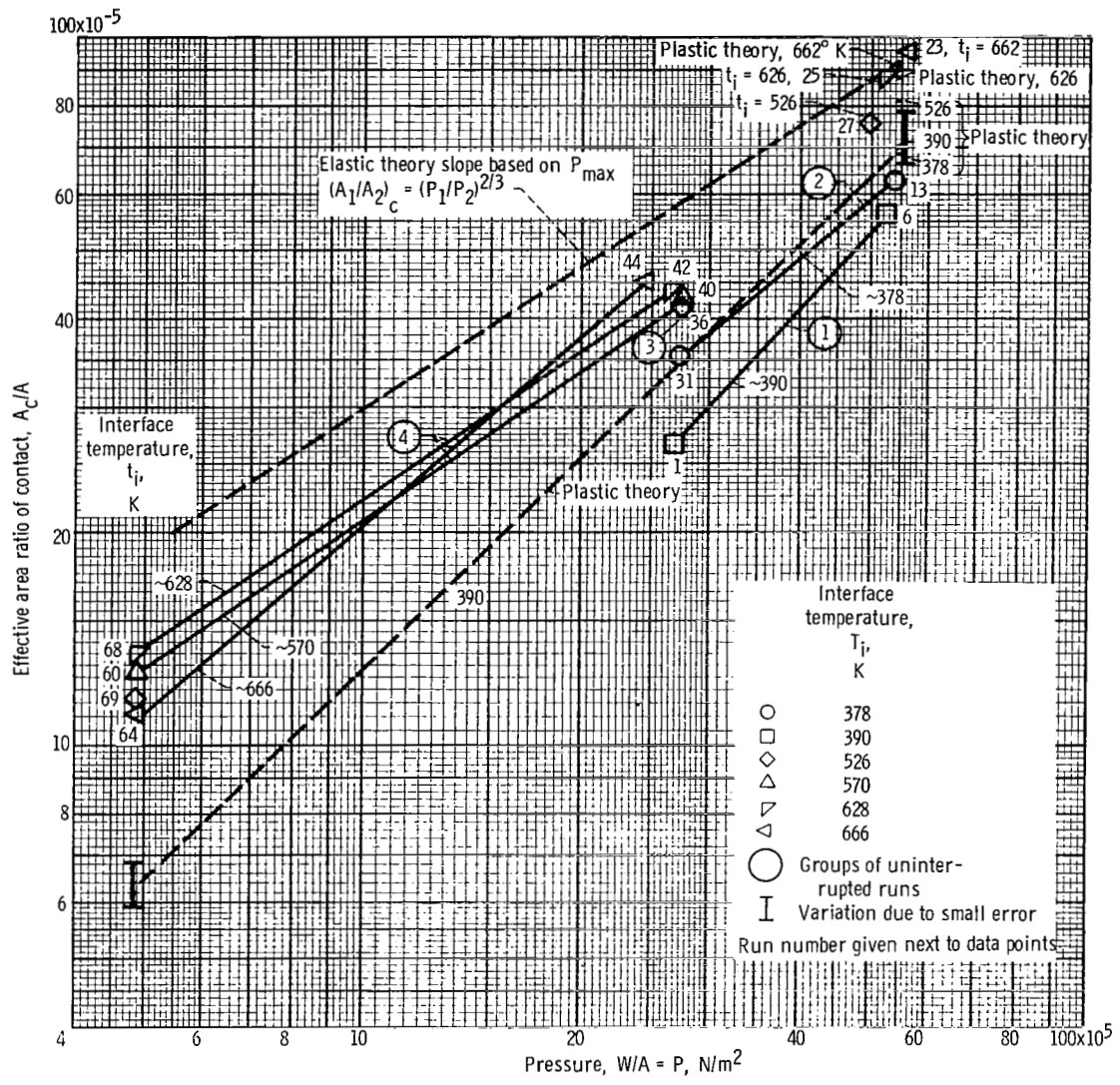


Figure 11. - Selected steady-state tungsten-tungsten data from figure 10. Data is grouped to eliminate effects of power interruptions. Effective area ratio of contact against pressure for ground surfaces with parallel lays. The arithmetic average roughness heights for the upper and lower surfaces were 0.538 and 0.943 micrometer, respectively.

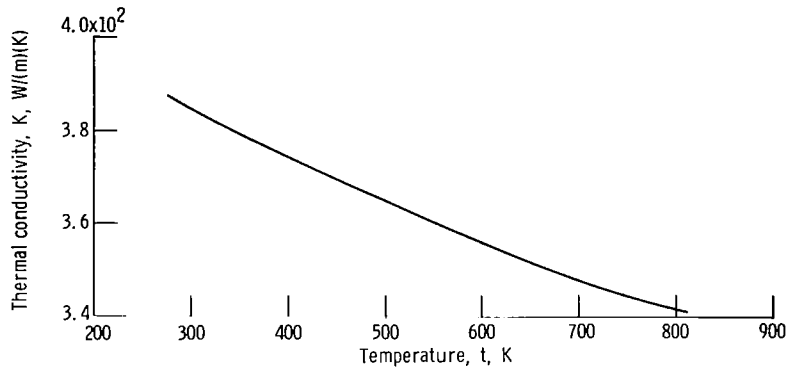


Figure 12. - Thermal conductivity of OFHC copper from reference 20.

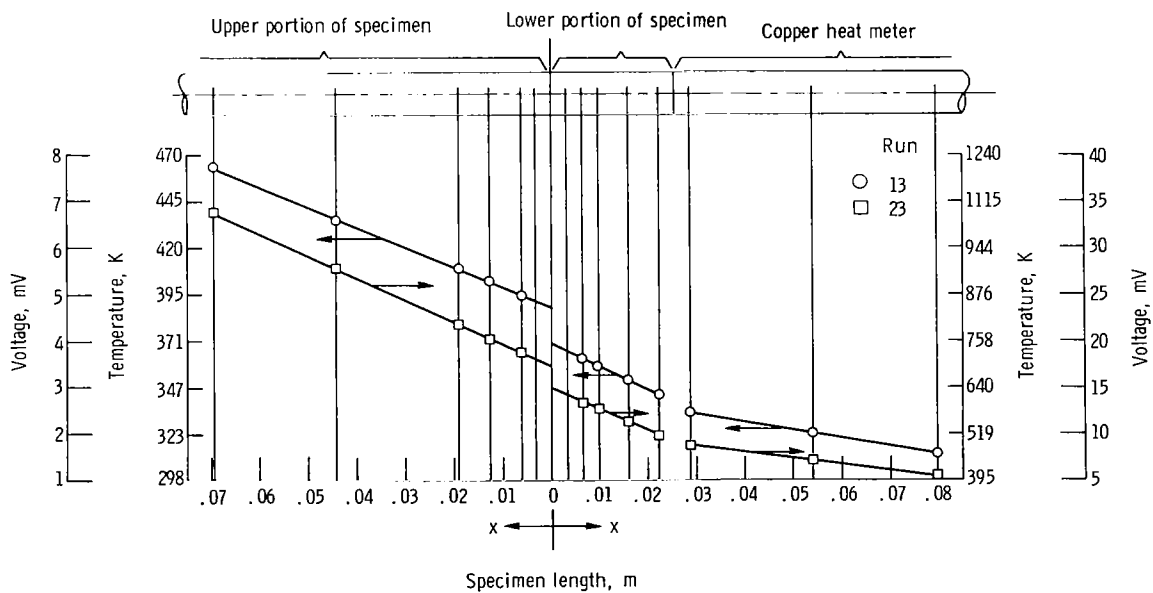


Figure 13. - Tungsten-tungsten specimen showing thermocouple location and data from typical runs 13 and 23.

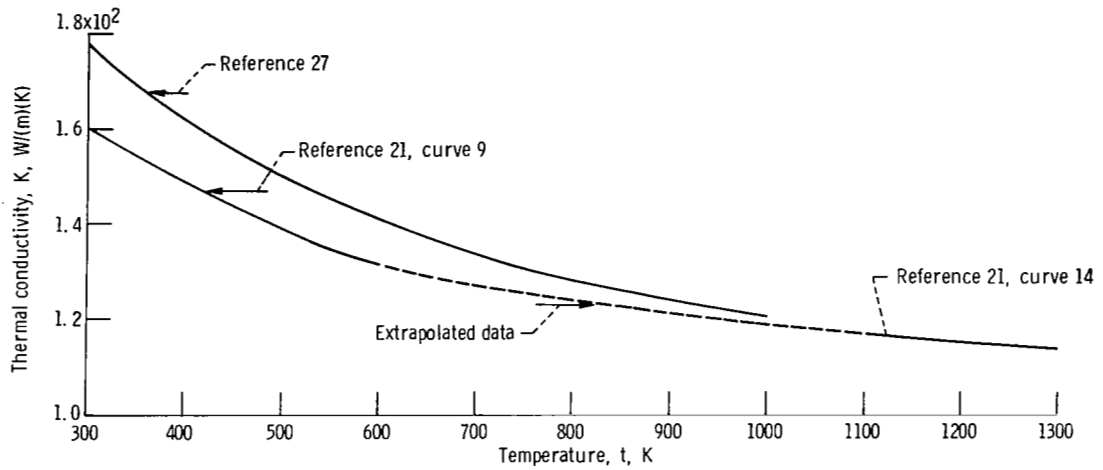


Figure 14. - Thermal conductivity of tungsten.

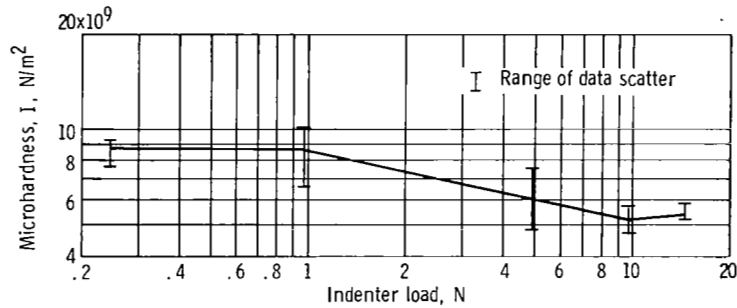


Figure 15. - Microhardness of interface surface of tungsten-tungsten specimen as function of indenter loadings at approximately 294 K.

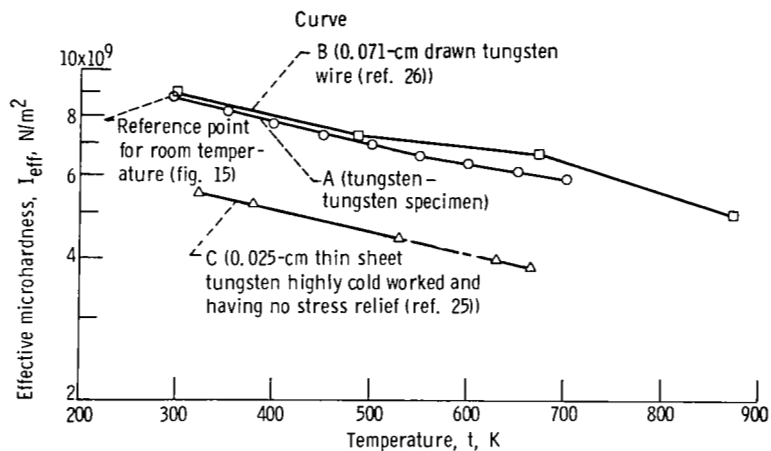


Figure 16. - Variation of tungsten-tungsten specimen effective microhardness as function of temperature computed using data from figures 8 and 15. Other tungsten hardness data are from references 25 and 26.